The Role of Oriented Attachment Crystal Growth in Hydrothermal Coarsening of Nanocrystalline ZnS

Feng Huang,* Hengzhong Zhang, and Jillian F. Banfield

Department of Earth and Planetary Science, University of California, Berkeley, California 94720-4767

Received: May 30, 2003; In Final Form: July 3, 2003

Approximately 2.0 nm diameter nanocrystalline zinc sulfide was synthesized in water (H_2O-ZnS) and ~2.4 nm nanocrystalline mercaptoethanol-capped ZnS was synthesized in a mercaptoethanol−water solution (mer-ZnS) in order to investigate the connections between the crystal growth pathway and microstructure development under hydrothermal conditions in water. XRD, HRTEM, and kinetic modeling were used to analyze reaction progress, determine the growth mechanism, and identify microstructural features. XRD and HRTEM data indicate that the H_2O-ZnS particles often contain planar defects, but these are uncommon in the initial mercaptoethanol-capped samples. Kinetic modeling and HRTEM data indicate that early crystal growth of both H_2O-ZnS and mercaptoethanol-capped ZnS occurs predominantly via crystallographically specific oriented attachment (OA). Twins and stacking faults form in the coarsened mercaptoethanol-capped ZnS, whereas more complex, closely spaced twins, stacking faults, and polytypic intergrowths are characteristic of coarsened H_2O-ZnS. These defects are consistent with those predicted for OA-based growth involving the microstructurally distinct initial particles. At longer reaction times, diffusion-controlled growth removes surface irregularities arising from OA to yield rounded particles with complex internal structures.

Introduction

The behavior of nanoparticles, especially the processes and products of crystal growth, are important in both materials and Earth sciences.[1] Semiconductor nanoparticles exhibit a wide range of size-dependent properties. Variations in fundamental characteristics, ranging from phase stability to electronic structure, can be influenced by the size and surface energy of the nanoparticles.[2,3] The unique size-dependent properties (e.g., quantum size effects) of nanometer-scale semiconductor crystallites such as CdS, CdSe, and ZnS have been extensively studied for potential materials applications.[2] For example, there has been great interest in their extremely enlarged third-order nonlinear susceptibility relative to bulk material[4] and the unusual luminescence properties[5] induced by quantum size effects. Nanocrystalline ZnS is also formed as a product of microbial sulfate reduction in Zn-enriched environments near Earth's surface.[6]

Understanding the factors that affect crystal growth kinetics and microstructure development in nanocrystals is fundamental to control of nanoparticle properties and determination of reactivity.[1,7−9] Typically, crystal growth kinetics have been studied using either micrometer- or nanometer-sized crystals. In most existing kinetic models, coarsening is described by Ostwald ripening,[10−13] in which crystal growth is controlled by diffusion. In these models, the kinetics of crystal growth strongly depend on the structure of the material, the properties of the solution, and the nature of the interface between the crystals and the surrounding solution. Since all of the contributing factors are independent of crystal size, Ostwald ripening models assume that the crystal growth mechanism is applicable to all length scales. However, a nanocrystal is tens to thousands of times larger than a small molecule but far smaller than a macroscopic crystallite. Thus, it is possible that the kinetics of reactions involving nanocrystals may share some characteristics with molecular reactions. Penn and Banfield reported a new crystal growth phenomenon in nanocrystalline TiO_2 that they referred to as oriented attachment.[14,15] OA-based growth was subsequently described in other materials, including FeOOH[16] and CoOOH.[17] In this process, adjacent particles orient so as to share a common crystallographic orientation. Subsequent elimination of the interface between them results in formation of a larger single crystal. Initially, the product retains an irregular shape that reflects formation from two individual particles. Microstructures are often byproducts of OA-based crystal growth. In particular, dislocations and planar defects are often a direct consequence of OA, and mark the region where initial particle−particle contact occurred.[14]

In a previous paper, we presented a kinetic model for OA crystal growth during hydrothermal coarsening of mercaptoethanol-capped ZnS nanocrystals.[18] In this paper we investigate hydrothermal crystal growth and microstructure development in water-synthesized nanocrystalline ZnS (H_2O-ZnS) and compare this to growth of organically capped ZnS. ZnS is of interest because its high symmetry should increase the probability of the OA growth process, which depends on achieving structural coherence between adjacent nanoparticles. The results of this work are relevant to materials science because novel particle morphologies and defect microstructures can be achieved via OA-based crystal growth, and to Earth science, where the crystal growth process determines the form and fate of biomineralization products over long time scales.

Experimental Section

The initial mercaptoethanol-capped nanocrystalline ZnS used in this study was synthesized using Vogel's method.[19] Briefly, sodium sulfide aqueous solution was dropped into equimolar zinc chloride aqueous solution in the presence of 0.1 M

* Corresponding author. Tel: 510 643 9120. E-mail: fhuang@eps.berkeley.edu.

10.1021/jp035518e CCC: $25.00
Published on Web 08/21/2003

mercaptoethanol at pH 10.2. Dissolved mercaptoethanol and excess synthesis reagents and products (NaCl) were removed by dialysis (until the pH was ~8.0 and Cl^- was below 1.77×10^{-9} M). The sample retained surface-bound mercaptoethanol, as demonstrated by the generation of H_2S upon heating in a quartz vacuum tube at 550°C. The initial nanocrystalline H_2O-ZnS used in this study was synthesized by a typical procedure where 2.95 g of $Zn(NO_3)_2 \cdot 6H_2O$ was added to 100 mL of deionized water. The pH was adjusted to 10.3 with 0.10 M NaOH. Then 0.8 g of Na_2S was added to the basic mixture, followed by 1 L of water. The solution was stirred for 10 min to ensure complete reaction. The white ZnS precipitate was filtered from solution and dried in a glass desiccator.

The H_2O-ZnS and mercaptoethanol-coated nanocrystalline ZnS were coarsened in aqueous solution at 140−225 °C and 3.6−25 bar in hydrothermal bombs. For time series experiments, samples of the same batch of ZnS were coarsened in separate hydrothermal vessels and sacrificed for analysis after different periods of time. X-ray diffraction (XRD) was used to identify the crystal structures and average particle sizes of initial and coarsened samples. Diffraction data were recorded using a Scintag PADV diffractometer with Cu Kαradiation (35 kV, 40 mA) in the step scanning mode. The 2θ scanning range was from 15° to 90° in steps of 0.02° with a collection time of 4 s per step. The average crystallite size was calculated from the peak broadening using the Scherrer equation. High-resolution transmission electron microscopy (HRTEM) was used to confirm the particle size and to determine the particle morphology. Approximately 10 HRTEM images of nanoparticles in zone axis orientations were recorded from the initial sample and each of the coarsened materials in order to evaluate the distribution of cubic and hexagonal ZnS structures and to identify the microstructures present. Samples were prepared for HRTEM study by dispersing the ZnS powder onto a holey carbon-coated Formvar support. HRTEM analyses were performed using a Philips CM200 UltraTwin HRTEM.

Results

Analysis of the Initial H_2O-ZnS and Mercaptoethanol-Capped ZnS. The experimental XRD patterns for initial nanocrystalline H_2O-ZnS is presented in Figure 1a and for mercaptoethanol-capped ZnS in Figure 1b. The average sizes of the particles were calculated from the peak broadening after subtraction of the instrumental contribution. Results indicated that the average size of H_2O-ZnS is ~2.0 nm and of mercaptoethanol-coated ZnS is ~2.4 nm.

At low pressure, ZnS can occur either as the cubic (sphalerite) or hexagonal (wurtzite) polymorph, or as a complex intergrowth of these (a polytypic mixture). Figure 1a shows three curves for spherical 2.0 nm ZnS calculated using the Debye function.[19] Curve I is for sphalerite, curve II is for wurtzite, and curve III is the best fit to the data achieved using 45% curve I + 55% curve II. The results suggest that the initial H_2O-ZnS sample contains more hexagonal stacking layers or wurtzite particles than the initial mercaptoethanol-capped sample. However, from this analysis it is impossible to determine whether the sample consists of a mixture of 45% sphalerite and 55% wurtzite particles or is a mixture of pure sphalerite and polytypic intergrowths of sphalerite and wurtzite.[18,19]

Figure 1b shows three curves for spherical 2.4 nm ZnS calculated using the Debye function.[19] Curve I is for sphalerite, curve II for wurtzite, and curve III is the best fit to the experimental data, achieved using 70% curve I + 30% curve II, suggesting that the mercaptoethanol-capped ZnS contains 30% wurtzite in some form.

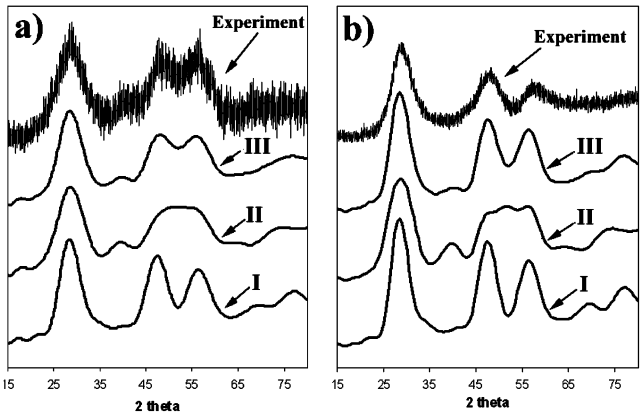

Figure 1. (a) Experimental diffraction pattern of initial nanocrystalline H_2O-ZnS compared with calculated diffraction curves for (I) 2.0 nm spherical sphalerite; (II) 2.0 nm spherical wurtzite structure; (III) 45% curve I + 55% curve II. (b) Experimental diffraction pattern of initial mercaptoethanol-capped nanocrystalline ZnS compared with calculated diffraction curves for (I) 2.4 nm spherical sphalerite; (II) 2.4 nm spherical wurtzite; (III) 70% curve I + 30% curve II.

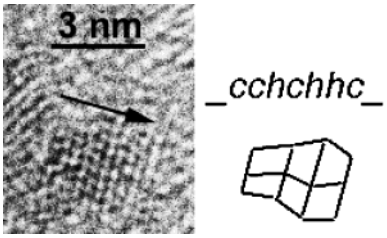

Figure 2. HRTEM image of a nanoparticle in the initial mercaptoethanol-capped ZnS sample. The stacking sequence determined from this image is indicated.

TEM-Based Structural and Microstructural Analysis of the Initial Samples. The HRTEM results indicate the presence of a wide variety of microstructures in the coarsened ZnS. We use the following terminology to describe the twins, stacking faults, and other disordered intergrowths that were detected. We use *c* to refer to a layer that is sandwiched by two different layers, and *h* to describe a layer that is sandwiched by two layers of the same type. Thus, cubic stacking ABCABC corresponds to *_cccc_* and hexagonal stacking, ABABAB, corresponds to *_hhhh_* ("_" indicates layers for which no determination can be made). A stacking fault in sphalerite, ABCABABC, is described as *_ccchhc_*. Note that the first *h* is bounded by layers with different designations (i.e., *chh*) but it is not a *c* because the convention refers to the actual layer position (ABA).

High-resolution transmission electron microscopy (HRTEM) showed that most particles in the initial mercaptoethanol-capped ZnS are pure sphalerite. However, Figure 2 shows a HRTEM image of a ZnS particle in which the close-packed layer-stacking sequence in the direction indicated by the arrow is *_cchchhc_* The initial nanocrystalline H_2O-ZnS particles formed such tight aggregates that it was impossible to clearly image a single particle via HRTEM.

HRTEM observation of OA in mercaptoethanol-capped and H_2O-ZnS in hydrothermally coarsened samples

Figure 3a shows a HRTEM image of a typical H_2O-ZnS nanoparticle coarsened at 140 °C for 110 h. Like many of the particles in this sample, this crystal has a highly irregular shape with rounded protrusions separated by indentations (see arrows), many of which are marked by planar defects. These features suggest that the particles were constructed from smaller primary particles, some of which appear to have been close in size to

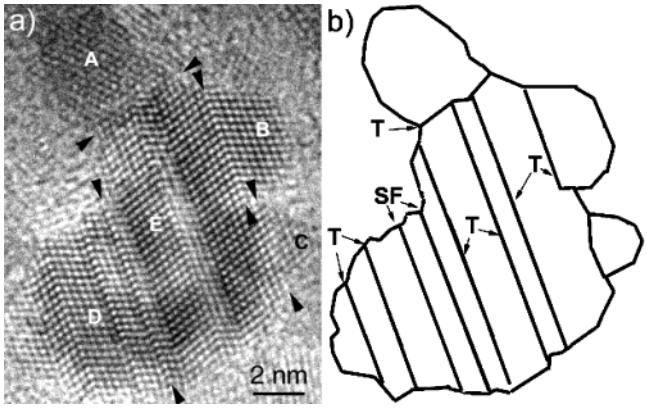

Figure 3. (a) HRTEM image of a crystal of H_2O-ZnS after hydrothermal coarsening at 140 °C for 110 h. The crystal is interpreted to have formed from several primary particles (e.g., regions A−E). Arrowheads mark possible interfaces between primary particles. (b) A diagram illustrating the key features of the crystal in Figure 3a.

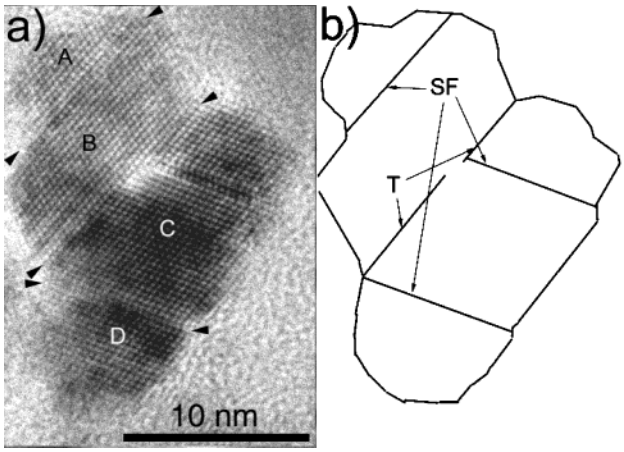

Figure 4. (a) HRTEM image of a complex ZnS crystal in the mercaptoethanol-capped nanocrystalline ZnS hydrothermal coarsened at 225 °C for 4 h. Arrowheads mark indentations, interpreted to be interfaces between primary particles. (b) A diagram illustrating key features in Figure 4a (rounded surfaces and defects) that are consistent with growth of this crystal via oriented aggregation of a number of primary particles.

the starting material. Figure 3b shows a diagram illustrating key features. Lattice fringe details in Figure 3a indicate that the interfaces between regions A and E and B and E are twins (T), whereas the interfaces between regions D and E are stacking faults (SF). Regions C and E are distinguished by difference in contrast due to thickness. If they represent distinct primary particles, they are in the same orientation.

Figure 4a shows a HRTEM image of a mercaptoethanol-capped ZnS sample coarsened at 225 °C for 4 h. As discussed for the H_2O-ZnS, surface features suggest that this crystal formed by oriented aggregation of several primary particles about <10 nm in diameter. This interpretation is illustrated in Figure 4b. Lattice fringe details in Figure 4a indicate that the interface between regions A and B, as well as between regions C and D, are stacking faults (SF), whereas the interface between regions B and C is a twin (T). The terminating stacking fault at the top of region C is associated with a partial dislocation near the center of the crystal.

HRTEM Data Illustrating the Phase Transition and Crystal Growth in Hydrothermally Coarsened Mercaptoethanol-Capped and H_2O-ZnS. Figures 5 and 6 are typical HRTEM images of H_2O-ZnS coarsened at 140 °C for 6 h and 110 h, respectively. After 6 h of coarsening, the particles

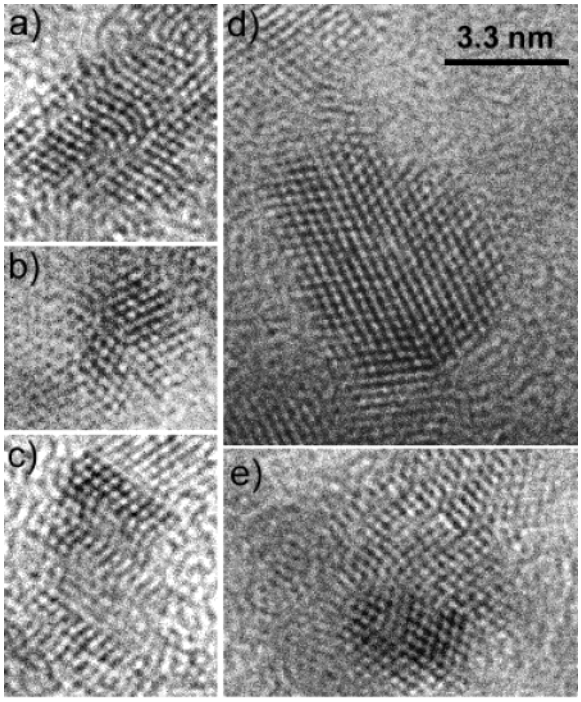

Figure 5. A series of typical HRTEM images of H_2O-ZnS coarsened at 140 °C for 6 h. (a) A particle containing polytype structures (PS). (b) OA of two small particles. (c) A particle containing polytype structures (PS) or paired twins (TT). (d) An image of a twined sphalerite particle. (e) Particle with many twins (T).

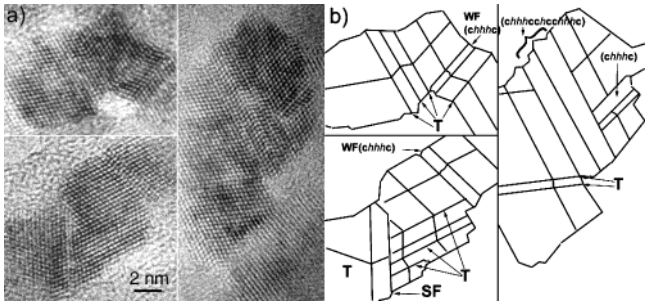

Figure 6. (a) A series of typical HRTEM images of H_2O-ZnS coarsened at 140 °C for 110 h. (b) Corresponding diagrams illustrating twins (T), wurtzite faults (WF), polytype structures (PS), and stacking fault (SF) in particles.

exhibit very complex structures. Some contain a single twin (*...ccchccc...*), some two twins (*...ccchchcc...*), others exhibit complex polytypic structures. After 110 h (Figure 6), the particles still exhibit irregular shapes and contain many twins, wurtzite faults (e.g., *...ccchhhcc...*), and polytype structures (e.g., *...cchhchc...*). Some of the complex polytypic structures do not appear to correspond with indentations suggestive of OA interfaces, and the separation between planar defect structures (e.g., a twin and stacking fault) is ~1 to 4 layers (0.31 nm to 1.25 nm), which is smaller than the average initial particle size 2.0 nm. In general, wurtzite packets were distributed within sphalerite and not as separate particles.

Figures 7 and 8 are typical HRTEM images of mercaptoethanol-capped ZnS coarsened at 225 °C for 32 h and 120 h, respectively. The majority of each particle is sphalerite. Wurtzite (several unit cells) appears on some surfaces, but was never observed within the crystals. Twins and stacking faults are common. Comparison between Figures 7 and 8 shows that with the increasing coarsening time the particles grow, but the volume of wurtzite does not change significantly. No pure wurtzite

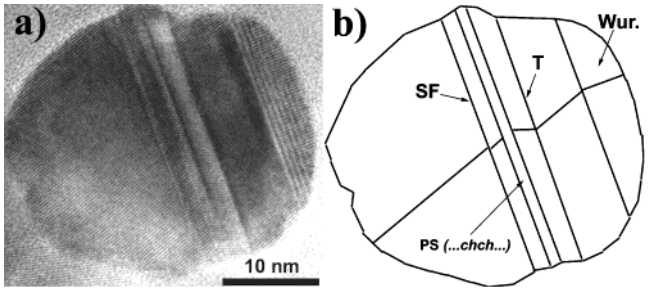

Figure 7. (a) A typical HRTEM image of mercaptoethanol-capped ZnS samples coarsened at 225 °C for 32 h. (b) A diagram illustrating the wurtzite (Wur) phase, polytype structure (PS), stacking faults (SF), and position of twins (T) in the particle.

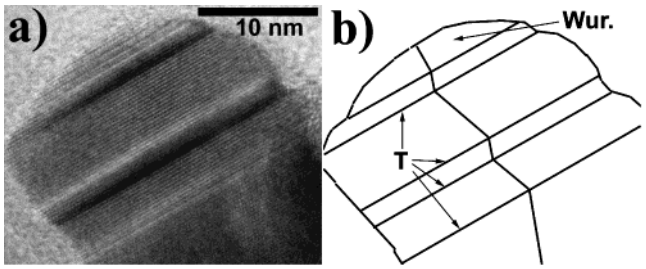

Figure 8. (a) A typical HRTEM image of mercaptoethanol-capped ZnS samples coarsened at 225 °C for 120 h. (b) A diagram illustrating the wurtzite (Wur) phase and position of twins (T) in the particle.

nanoparticles were ever found in HRTEM images from any of the coarsened mercaptoethanol-capped samples.

Discussion

Coarsening Kinetics. Our previous work showed that the coarsening kinetics of mercaptoethanol-stabilized ZnS nanoparticles can be divided into two steps. At the beginning of the hydrothermal treatment the mercaptoethanol capping limits diffusion of ions, thus prevents particle coarsening via Ostwald ripening. Thus, in the first step, the coarsening is controlled by OA and the growth curve can be fit by an OA kinetic equation (eq 1):[18]

$$D = \frac{D_0(\sqrt[3]{2}k_1t + 1)}{(k_1t + 1)} \tag{1}$$

where D is the particle diameter at any time, D_0 is the initial particle diameter, k_1 is the rate constant for OA, and t is time. The activation energy of OA is $E_a(k_1) = 136.8 \pm 9.1$ J/mol.

The second step of crystal growth was fit using an equation based on that for Oswald ripening:[18]

$$D - D_2 = k_2(t - t_2)^{1/n} \tag{2}$$

where D_2 is the average diameter at the beginning of the second stage and t_2 is the time of onset of the second stage, and n is a constant equal to 3. The activation energy derived from this fit is $E_a(k_2) = 41.8 \pm 5.9$ J/mol. Note that this is an apparent value and cannot be interpreted as an activation energy for Ostwald ripening because the HRTEM data clearly show that both OA and Ostwald ripening are important in the second stage.

In this work, we analyzed the coarsening kinetics for ZnS nanoparticles that were synthesized and coarsened in water (no mercaptoethanol). Figure 9a−d shows the increase in average particle size vs time at temperature of 140 °C, 175 °C, 200 °C, and 225 °C. The data cannot be fit with eq 1 or eq 2 separately. However, the data can be fit by an equation that considers that the particle size at any time is the result of the two processes occurring simultaneously (i.e., by substituting D_2 in eq 2 with the D in eq 1 and with $t_2 = 0$ in eq 2):

$$D = \frac{D_0(\sqrt[3]{2}k_1t + 1)}{(k_1t + 1)} + k_2t^{1/n} \tag{3}$$

Note that the component of growth described by the first term (describing pure OA growth) diminishes rapidly so that the second term predominates over longer times. The activation energy of OA is $E_a(k_1) = 125.0$ J/mol, and the activation energy for the hybrid component described by the second term in eq 3 is $E_a(k_2) = 42.4$ J/mol. These two activation energies are comparable with those determined previously for the mercaptoethanol-capped sample.

Equation 3 can provide only a limited illustration of the physical process for two reasons. First, the simplification in its derivation is that the two processes occur simultaneously but do not affect each other. Second, it is based on eq 2, which was derived for pure Ostwald ripening but describes crystal growth kinetics that occur via a combination of the pathways. However, in general terms, the fit suggests that at the beginning of the coarsening, OA crystal growth dominates (see thick lines in Figure 9a−d). The H_2O−ZnS sample coarsened at 140 °C for 6 h (Figure 7) corresponds to this stage (Figure 9a). HRTEM data show that the coarsened particles are irregular in shape, with complex microstructures marking indentations interpreted to arise from joining of individual nanoparticles in crystallographically specific orientations. These observations support that conclusion that OA is the most important process occurring during early growth of nanocrystalline ZnS in water.

The fit to the experimental data using eq 3 suggests that with increasing time, hybrid crystal growth (Ostwald ripening and OA) becomes increasingly important (see thin lines in Figure 9a−d). The sample coarsened at 140 °C for 110 h (Figure 9) is from this stage. The particles are still not completely round. However, some parts of particles contain very complex microstructures, whereas other parts are microstructure-free and appear to have formed by overgrowth of the initial particles via diffusion-based growth. TEM data showing very rounded particles at long reaction times suggest that Ostwald ripening eventually becomes the only significant crystal growth pathway.

The mercaptoethanol-capped sample coarsened at 225 °C for 32 h and 120 h are from the second, hybrid crystal growth stage.[18] HRTEM images show that the particles have relatively smooth edges and round or elliptical shapes and large domains of perfect sphalerite occur (see Figures 5 and 6). These results suggest that Ostwald ripening dominates in these samples.

Phase Transition and Crystal Growth Morphology. HRTEM images show that the microstructure of coarsened H_2O−ZnS samples is complex. Paired twins (TT), wurtzite faults (WF), and polytype structures (PS) are present. In contrast, the coarsened mercaptoethanol-capped samples are relatively microstructurally simple. Most of the particles are pure sphalerite, but some contain wurtzite (only on the surface). Although the coarsened mercaptoethanol-capped particles display stacking faults (SF) and twins (T), wurtzite fault (WF) and polytype structures (PS) are seldom found (see Figures 5 and 6).

The above kinetic analysis indicates that the OA crystal growth mechanism dominates, regardless of whether the initial sample is mercaptoethanol-capped or surrounded only by water. Figure 10 illustrates all the possible structures that can be generated when two pure sphalerite particles grow via OA. Only defect-free sphalerite, twins (...*cchcc*...), and stacking faults

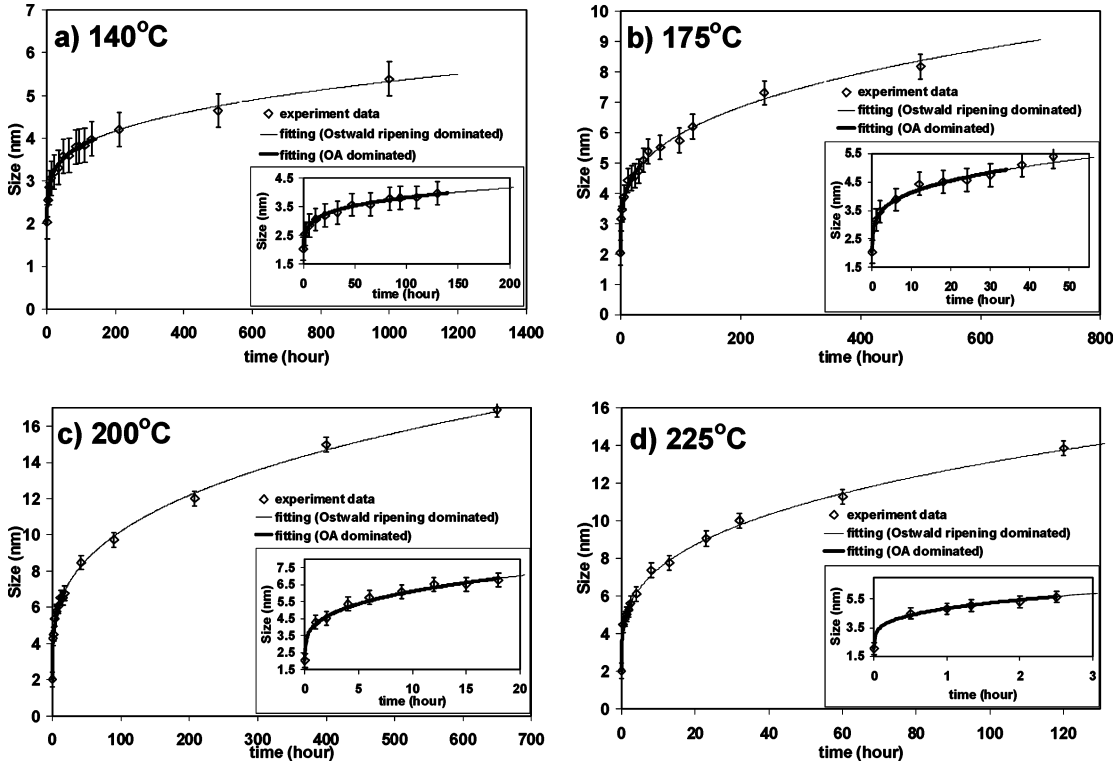

Figure 9. Experimental data and fitting results for particle sizes vs time at each temperature, insets are enlarged plots for OA-dominated coarsening.

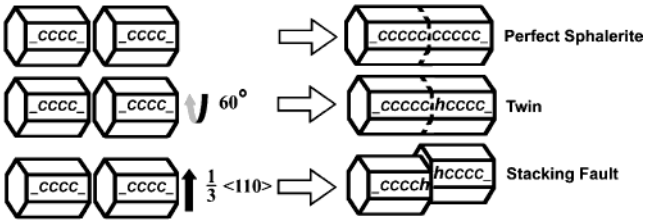

Figure 10. Illustration of all the possible structures produced by OA crystal growth involving two defect-free sphalerite particles. The "_" on the sphalerite surface is undefined until the layer is bounded on both sides by ZnS layers. This occurs as the result of OA. The two particles can form a coherent interface in one of three ways. The first results in a perfect crystal; the second generates a twin (...*cchcc*..., i.e., the particles are superimposed such that the stacking sequence is rotated by 60° at the interface); the third generates a stacking fault (...*cchhcc*..., i.e., the second particle is shifted by 1/3 ⟨110⟩ relative to the first). All other translations or rotations are symmetrically equivalent.

(...*cchhcc*...) can be formed. Paired twins (TT), wurtzite fault (WF), and polytype structures (PS) cannot be formed. Note that the distance between T and SF formed directly by OA involving defect-free sphalerite particles should not be smaller than the initial size of the particles. However, structures containing closely spaced defects could be created via OA if the initial particles are polytypically complex.

Figures 7 and 8 show that the interval between two planar defect structures (T and SF) in the H_2O-ZnS sample ranges between ~1 and 4 layers (0.312 nm to 1.248 nm), thus is smaller than the average initial particle size (~2.0 nm). This implies that these defects formed by OA involving initial particles that contained planar defects prior to coarsening.

For coarsened mercaptoethanol-capped samples, the distances between two layer fault structures (T and SF) are typically larger than the initial particle size. This is consistent with growth involving initial ZnS particles that are essentially free of planar defects. XRD analysis verified that there is more wurtzite-type stacking in the H_2O-ZnS initial sample than in the mercaptoethanol-coated sample, explaining the formation of the more complex polytype structures as the result of OA growth only in the H_2O-ZnS sample.

In the coarsened mercaptoethanol-capped samples, pure sphalerite particles are common and no independent pure wurtzite particles were detected via HRTEM. However, wurtzite appears on the surfaces of some coarsened particles. This suggests that wurtzite may be formed as the result of diffusion-based growth, possibly due to stabilization of wurtzite relative to sphalerite at small particle sizes and these temperatures.

Conclusions

Hydrothermal coarsening and microstructure development of H_2O-ZnS has been analyzed using XRD and HRTEM, and results compared with those from mercaptoethanol-capped samples. HRTEM evidences for OA-based crystal growth were observed in both mercaptoethanol-capped and H_2O-ZnS. The kinetic investigation of the coarsening process suggests that OA-based crystal growth dominates when the particle size is small, both for mercaptoethanol-capped ZnS and H_2O-ZnS. The microstructures in coarsened H_2O-ZnS can be explained in terms of OA involving the planar defect-bearing primary particles. In contrast, twin and stacking fault microstructures developed in the coarsened mercaptoethanol-capped ZnS can be attributed to oriented attachment-based growth involving relatively defect-free particles.

Acknowledgment. Financial support for this study was provided by grants from the National Science Foundation Grant EAR-9814333, the Department of Energy Basic Energy Sciences Program Grant DE-FG03-01ER15218, and Lawrence Berkeley National Laboratory LDRD program. Transmission electron microscope characterization was conducted in the Materials Science Center, University of Wisconsin−Madison. We thank Mr. Michael Finnegan for providing assistance with the use of hydrothermal and XRD equipment and Michael Finnegan, Ben Gilbert, and Glenn Waychunas for discussion.

References and Notes

(1) *Reviews in Mineralogy & Geochemistry, Vol. 44: Nanoparticles and the Environment*; Banfield, J. F., Navrotsky, A., Eds.; Geochemical Society and Mineralogical Society of America, Washington, DC, 2001.

(2) Alivisatos, A. P. *J. Phys. Chem.* **1996**, *100*, 13226.

(3) Huang, F.; Gilbert, B.; Zhang, H.; Banfield, J. F. *Phys. Rev. Lett.*, submitted.

(4) Jain, R. K.; Lind, R. C. *J. Opt. Soc. Am.* **1983**, *73*, 647.

(5) Empedocles, S. A.; Bawendi, M. G. *Science* **1997**, *278*, 2114.

(6) Labrenz, M.; Druschel, G. K.; Thomsen-Ebert, T.; Gilbert, B.; Welch, S. A.; Kemner, K. M.; Logan, G. A.; Summons, R. E.; Stasio, G. D.; Bond, P. L.; Lai, B.; Kelly, S. D.; Banfield, J. F. *Science* **2000**, *290*, 1744.

(7) Efros, Al. L.; Efros, A. L. *Sov. Phys. Semicond.* **1982**, *1*6, 772.

(8) Ekimov, A. I.; Onushchenko, A. A. *Sov. Phys. Semicond.* **1982**, *1*6, 775.

(9) Brus, L. E. *J. Chem. Phys.* **1983**, *7*9, 5566.

(10) Lu, K. *Mater. Sci. Eng.* **1996**, *R16*.161.

(11) Kirchner, H. O. K. *Metall. Trans.* **1971**, *2*, 2861.

(12) Speight, M. V. *Acta Metall.* **1968**, *16*, 133.

(13) Wagner, C. *Z. Elektrochem.* **1961**, *65*, 581.

(14) Penn, R. L.; Banfield, J. F. *Science* **1998**, *281*, 969.

(15) Penn, R. L.; Banfield, J. F. *Am. Mineral.* **1998**, *83*, 1077.

(16) Penn, R. L.; Oskam, G.; Strathmann, G. J.; Searson, P. C.; Stone, A. T.; Veblen, D. R. *J. Phys. Chem. B* **2001**, *105*, 2177.

(17) Penn, R. L.; Stone, A. T.; Veblen, D. R. *J. Phys. Chem. B* **2001**, *105*, 4690.

(18) Huang, F.; Zhang, H.; Banfield, J. F. *Nano Lett.* (*communication*) **2003**, *3*, 373.

(19) Vogel, W.; Borse, P. H.; Deshmukh, N.; Kulkarni, S. K. *Langmuir* **2000**, *16*, 2032.